ELSEVIER

Contents lists available at ScienceDirect

Chemical Engineering Journal Advances

journal homepage: www.sciencedirect.com/journal/chemical-engineering-journal-advances





Engineering waveguide surface by gradient etching for uniform light scattering in photocatalytic applications

Xiangkun Elvis Cao ^{a,1}, Tao Hong ^b, Spencer Hong ^c, David Erickson ^{a,*}

- a Sibley School of Mechanical and Aerospace Engineering, Cornell University, Ithaca, NY 14853, United States
- b Department of Materials Science and Engineering, Cornell University, Ithaca, NY 14853, United States
- ^c Smith School of Chemical and Biomolecular Engineering, Cornell University, Ithaca, NY 14853, United States

ARTICLE INFO

Keywords: Gradient etching Uniform scattering Glass waveguide Optofluidics Photoreactor

ABSTRACT

In photoreactors, non-uniform light distribution leads to regions either with an overabundance of light or insufficient light irradiation. The integration of light-guiding elements such as waveguides into photocatalytic reactors has been an emerging approach to improve light delivery. However, traditional waveguides with constant surface properties experience an exponential decay in scattering light intensity under side irradiation. This reduces the light propagation length and hinders the scale-up potential. In this work, we derive the relationship between attenuation coefficients with etching time, determine the correlation between etching time and waveguide location for uniform scattering, and experimentally validate different light scattering profiles by engineering the surface roughness distribution of waveguides. We apply a dimensionless number, the coefficient of variation, to characterize the relative light distribution uniformity for gradient-etched, uniform-etched, and unmodified waveguides. Scattering light uniformity via gradient etching is more than 13 times higher than that for uniform-etching. In addition, the light distribution for gradient etching exhibits improved uniformity than other approaches, such as tip coating, physical carving, and engineered pillars. We then evaluate the effect of different light scattering profiles on photocatalytic activities in a photodegradation test for methylene blue, with non-etched, uniform-etched, and gradient-etched waveguides serving as internal light-guiding elements. Gradient-etched waveguides show ~4 times improvement in photodegradation activity over uniform-etched designs and ~8 times over non-etched configurations. This result underscores gradient etching for waveguides as a viable approach for precision light delivery to increase the light distribution uniformity, thus enhancing reaction rates for photocatalytic reactors.

1. Introduction

Photocatalytic reactions have been applied on various occasions, such as environmental remediation [1–3], photocatalytic CO_2 reduction [4–6], light-driven water splitting [7], and solar ammonia synthesis [8], etc. As the name "photocatalysis" indicates, light availability is the key to the efficiency of subsequent photoreactions. Uneven light distribution, therefore, is one of the challenges affecting photoreactors' performance: an overabundance of light leads to wasted photon energy due to the saturated photocatalytic reaction, and insufficient light irradiation cannot penetrate through the catalyst film and result in optically dark regions; thus catalyst is being underutilized [9–13].

The integration of light-guiding elements (e.g., waveguides) has

proved to improve light distribution (thus better photon utilization) [12, 14–18]. Waveguides can either serve as support structures for directly coating catalyst materials [17,19,20], or as internal illuminators for introducing scattered light to catalyst particles coated on other surfaces (e.g., in a monolith) [21–23]. However, light scattering intensity follows an exponential decay under side irradiation for waveguides with uniform surface properties (i.e., constant attenuation coefficients) [24]. The exponential intensity decay reduces the light propagation length and hinders the scale-up potential for photocatalytic reactors [25,26]. Thus, there is an urgent need to engineer the surface roughness distribution of waveguides to increase light scattering and its uniformity. Researchers attempted several physical and chemical approaches to modify the waveguide properties for enhanced light scattering by introducing

^{*} Corresponding author.

E-mail address: de54@cornell.edu (D. Erickson).

¹ MIT Climate & Sustainability Consortium (MCSC), Massachusetts Institute of Technology, Cambridge, MA 02139, USA.

surface scatterers (e.g., engineered pillars) [10,27,28], applying backscattering (e.g., dip coating) [21,29], and creating surface cracks (e.g., sandblasting, physical carving, chemical etching) [4,11,21], etc. Engineered pillars could enhance light emission and increase light distribution uniformity, but this process required complex equipment such as the contact aligner system [27,28]. Backscattering by tip coating could improve the amount of light scattering but would not affect light transmission uniformity [21]. Introducing surface cracks to waveguides was proved to increase scattering while increasing catalyst adhesion affinity [30]. A variety of techniques could create surface cracks: sandblasting [4], physical carving [21], and chemical etching [11], etc. Physical carving for waveguides usually involves a tedious manual process. Thus parameters affecting the surface engineering accuracy and consistency are hard to control. While sandblasting can be automated, it could only generate a uniform distribution of surface roughness along the waveguide. Compared with sandblasting and physical carving, chemical etching can be easily programmable to achieve a gradient distribution of surface roughness, thus offering the potential for precision control of waveguide surface engineering to enable uniform light scattering.

In this work, we presented gradient etching as a viable approach to precisely control the surface roughness distribution of waveguides for achieving uniform light scattering. We first established the relationship between attenuation coefficients with etching time. We then built a programmable etching set-up to apply various etching profiles to different waveguides. The light scattering behaviors for these waveguides were later characterized with a custom-built platform that could achieve automatic and continuous light measurement. We then examined the relative light distribution uniformity for waveguides etched by different configurations via a dimensionless performance metric. We compared it with other state-of-the-art approaches to increase light scattering uniformity. The effect of varying light scattering profiles on photocatalytic activities was validated in a photodegradation test for methylene blue, with non-etched, uniform-etched, and gradient-etched waveguides serving as internal light-guiding elements.

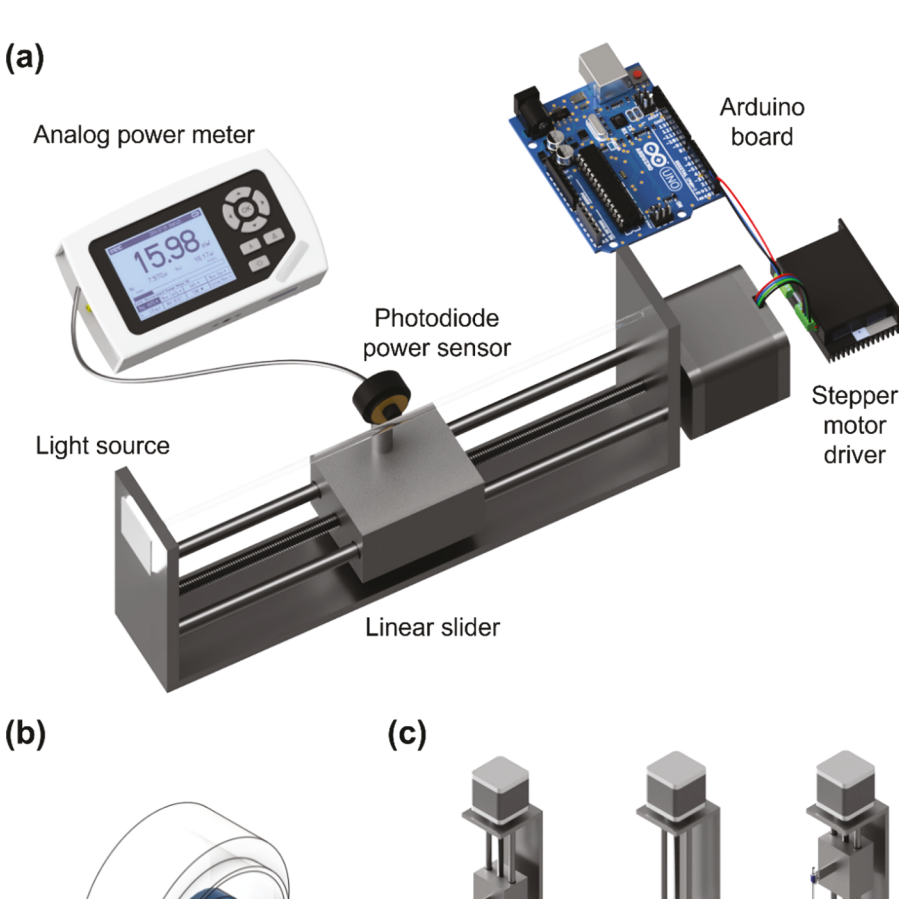


Fig. 1. (a) Schematic diagram of the linear-slider-based set-up for continuous scattering light measurement. Sizes are not to scale. Data collection on the computer is not shown for clarity. (b) Zoomed-in view for the photodiode power sensor. The aperture introduces scattering light to the photodetector. (c) Three stages of the gradient etching process: initialization, insertion, and withdrawal. The quartz waveguide moves with the linear slider under the control of an Arduino board. The Arduino board and other components are not shown for clarity.

2. Materials and methods

2.1. Design of light measurement and controlled etching systems

An optical power detector (Thorlabs) was attached to the linear slider. The motion of the linear slider was controlled by a stepper motor driver connected to an Arduino board (Fig. 1a). A rubber aperture was applied to collect only the scattering light from the adjacent waveguide to the photodetector (Fig. 1b). During the measurement, the glass rod was illuminated by a light-emitting diode (LED) operated at 30 W from the end. The light sensor coupled with the rubber aperture moved from one end of the glass rod to another to collect the scattering light automatically and continuously. The scattering light power was recorded by the analog power meter connected to the sensor, , and its intensity was then calculated by dividing the scattering light power by the area of the rubber aperture. The light measurement set-up's right side view and top view were presented in Fig. S1a and Fig. S1b, respectively.

The waveguides were fabricated from fused quartz rods (Technical Glass Products) and treated with a glass etchant (Armor Products). The quartz waveguides were 3 mm in diameter and were cut to desired lengths with a glass cutter. The etchant is a solution of sodium bifluoride and ammonium bifluoride in water. The controlled etching process includes three stages: initialization, insertion, and withdrawal (Fig. 1c). An Arduino board was programmed to control the linear slider to achieve different withdrawal speed at various locations for the etched waveguide.

2.2. Model development for uniform scattering

It is well established that in a homogeneous longitudinal waveguide, one would expect to get an exponential decay in the intensity of the illumination remaining in the waveguide [26].

$$I_{rod}(z) = I_{input}e^{-\alpha z} \tag{1}$$

where $I_{rod}(z)$ represents the amount of light remaining in the glass rod at any axial position z; I_{input} is the amount of light that enters the rod at the tip (z=0); and α is the attenuation coefficient. It depends on the optical and physical properties of the rod core and the surface coatings, if any.

If we assume the primary loss of light transmission in a glass rod is through scattering from the surface, then the relationship between the light scattered out of the rod, $I'_{scatter}(z)$, and the light remaining in the rod, $I_{rod}(z)$, is given by [25].

$$I_{scatter}'(z) = -\frac{dI_{rod}(z)}{dz}$$
 (2)

Substituting the expressions of $I_{rod}(z)$ from (1) into (2) gives

$$I_{scatter}'(z) = -\frac{d[I_{input}e^{-\alpha z}]}{dz} = \alpha I_{input}e^{-\alpha z} = \alpha I_{rod}(z)$$
(3)

This proves that the ratio between the amount of light scattering out of the rod and the light remaining in the rod is a constant at any position z, where α represents the localized surface property, the attenuation coefficient, and can be expressed as $\alpha(z)$. Since uniform-etched rod has uniform surface properties, thus $\alpha(z)$ is a constant under uniform etching. One could expect the light scattering to follow an exponential decay profile along the light transmission.

To achieve uniform scattering, $I'_{scatter}(z)$ needs to be a constant:

$$I'_{scatter}(z) = I'_{uniform} \tag{4}$$

Substituting (4) into (2), then I_{rod} (z), the amount of light remaining in the rod at position z becomes:

$$I_{rod}(z) = I_{input} - I_{uniform}'z$$
 (5)

This proves that to achieve a uniform scattering profile in the radial direction (i.e., constant $\Gamma_{scatter}$), we need to engineer a linear decay profile for $I_{rod}(z)$, the light transmission in the axial direction.

By substituting (4) and (5) into (3), the ratio between the amount of light scattered out and the amount remaining in the rod, $\alpha(z)$, is given by:

$$\alpha(z) = \frac{I^{'}_{scatter}(z)}{I_{rod}(z)} = \frac{I^{'}_{uniform}}{I_{input} - I^{'}_{uniform}z} = \frac{1}{\frac{I_{input}}{I^{'}_{uniform}} - z}$$
(6)

This proves that $\alpha(z)$ increases as z rises: indicating a smoother rod surface (lower α) closer to the light source and a rougher rod surface (higher α) further from the light source to achieve uniform scattering. It also proves that under a constant I_{input} , if uniform light scattering intensity (I'uniform) is high, then $\alpha(z)$ is high, indicating a shorter distance for light transmission.

Eq. (6) establishes the relationship between attenuation coefficient (α) with rod position (z) through $\alpha(z)$. Attenuation coefficient (α) , on the other hand, can be controlled by changing etching time (t) through the function of $\alpha(t)$. By equaling $\alpha(z)$ and $\alpha(t)$, we will be able to drive t(z). This provides a practical method to apply different etching time (t), thus different attenuation coefficients (α) , for various positions of the rod (z).

To determine $\alpha(t)$, we uniformly etched glass rods (diameter: 3 mm, length: 130 mm) for 6 different time intervals: 10, 20, 30, 40, 50 and 60 min, respectively. The attenuation coefficients for different etching time were then determined by exponentially fitting the scattering intensity profiles.

2.3. Design of a photocatalytic system based on surface-engineered glass waveguides

The photocatalytic system was constructed with a waveguidecoupled 250 mL glass flask (McMaster-Carr), with a 380 nm UV LED (Chanzon) serving as the light source from the top (Fig. S4b). The LED was set to operate at 30 W by a power control (BK Prevision), and a fan was kept on to take away excess heat by the LED.Light was only introduced into the solution by the waveguide, with the rest of the LED covered by an aluminum foil, so that no additional heat was introduced to the solution. The solution was maintained at room temperature at ~20 °C throughout the tests, as confirmed by temperature measurements of the solution after certain time intervals. An external light shielding covered the whole system with aluminum foil during photocatalytic tests. A magnetic stirrer hot plate mixer (Microvn) agitated continuously to achieve a homogeneous environment. For each photodegradation test, 0.25 g of TiO2 catalyst in rutile phase (US Research Nanomaterials) was added to a 250 mL methylene blue solution with an initial concentration of 5 x 10^{-6} M. The photodegradation efficiencies using different waveguides were compared after 1 h of irradiation. The degradation percentage was determined by analyzing its absorbance at 670 nm by an Ocean Optics HR4000 high-resolution fiber optic spectrometer (Fig. S4a). The spectrometer measured absorbance levels, and these values were correlated with their respective concentrations by a pre-defined calibration curve (Fig. S5).

3. Results and discussion

3.1. Relationship between attenuation coefficient and etching time

Under different etching durations, light scattering yielded different decay profiles, indicating different attenuation coefficients for the waveguide surface (Fig. 2a). The unstable scattering profile in the first 10 min could result from the non-uniform surface properties and initial cracks on the waveguides. After 10 min of etching, the attenuation coefficient was still low, which could be explained by the chemical reaction's initialization process between the etchant and rod surface. On raising the etching time from 10 min to 20 min, the attenuation

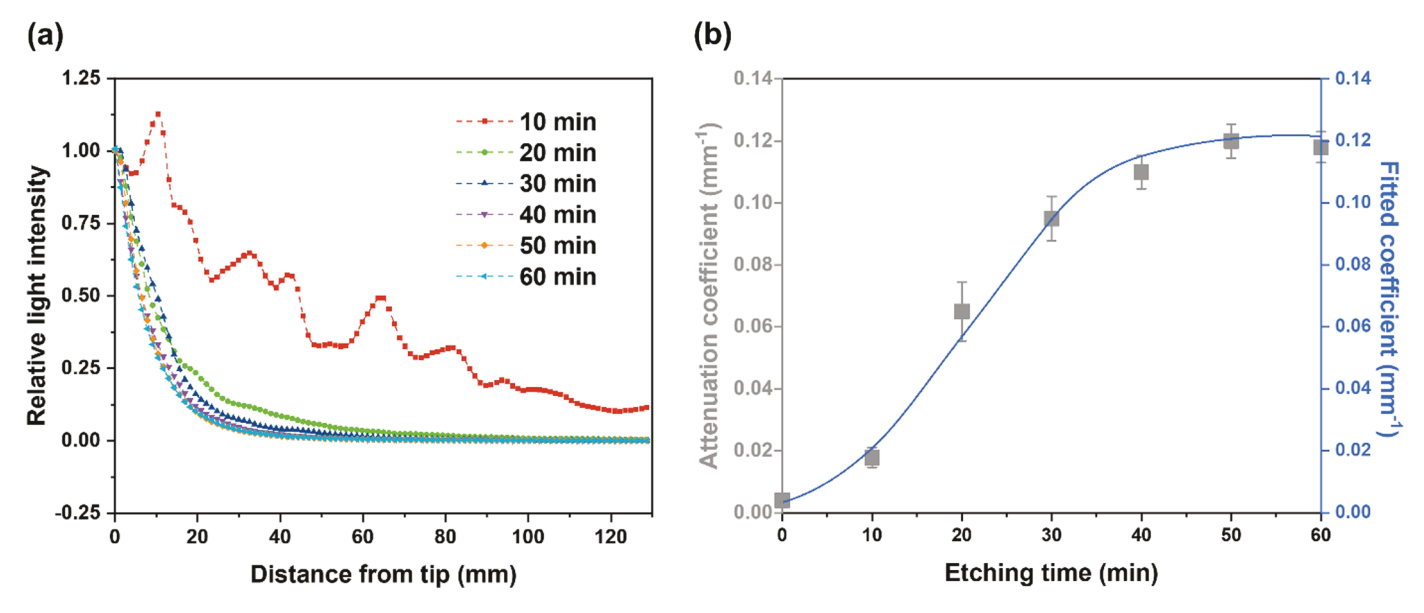


Fig. 2. (a) The change of relative scattering intensities versus the distance from the rod tip, under different etching durations (10 min, 20 min, 30 min, 40 min, 50 min, 60 min). As etching time increases, light scattering intensities decay faster. (b) The change of attenuation coefficients under different etching time. The gray square denotes the measured attenuation coefficients during experiments, and error bars represent the standard deviation calculated from three measurements. The blue line indicates the fitted coefficients using an error function. All experiments were conducted three times, and error bars were included only in (b) for clarity (For interpretation of the references to color in this figure legend, the reader is referred to the web version of this article.).

coefficient increased from 0.020 to 0.057 mm $^{-1}$. Along with the 2.8-fold increase in surface roughness, the scattering intensity distribution also became smoother, indicating more uniform surface properties. As the etching time rose to 30 min, the attenuation coefficient reached 0.095 mm $^{-1}$, around a 5-fold increase compared with that for 10 min, indicating a rapid growth for surface roughness during this period. From 30 min onward, the attenuation coefficient growth slowed down, with only a \sim 20% increase in the first 10 min interval and a \sim 5% increase in the second 10 min interval (Fig. 2b).

The surface roughness (i.e., attenuation coefficient) stabilized after 50 min of etching, evidenced by the fact that the curve for 50 min almost overlapped that for 60 min (Fig. 2a), and the attenuation coefficients for both 50 min and 60 min were close to 0.120 mm $^{-1}$ (Fig. 2b). The slow-fast-slow increase in attenuation coefficients resembled the shape of an error function, and the following fitting yield an R^2 value of 0.99, indicating a good correspondence:

$$\alpha(t) = c * erf \left[m(t - t_{half}) \right] + \alpha_{half}$$
(7)

where the values of constants were determined from the fitting function: $c=0.062~\mathrm{mm^{-1}},~m=0.062~\mathrm{mm^{-1}},~t_{half}=20.56~\mathrm{min},~\alpha_{half}=0.06~\mathrm{mm^{-1}}.$

3.2. Relationship between etching time and rod position

Eq. (6) proves the feasibility of generating a uniform light scattering distribution by engineering a gradient distribution of attenuation coefficients: a lower attenuation coefficient (i.e., lower etching time) closer to the light source and a higher attenuation coefficient (i.e., higher etching time) further from the light source. Considering the unstable scattering in the initial stages of etching Fig. 2a), the lowest etching time was set as 7.5 min through trial-and-error; thus, the attenuation coefficient at the tip (z = 0) is determined as 0.014 mm⁻¹ from Eq. (7). The etching time as a function of rod position t(z) is obtained by equaling $\alpha(z)$ and $\alpha(t)$, by combining Eqs. (6) and ((7):

$$\frac{1}{T_{input}} - z = c * erf \left[m \left(t - t_{half} \right) \right] + \alpha_{half}$$
(8)

By solving this equation, the corresponding etching time as a function of

location is:

$$t(z) = erfinv \left[\left(\frac{1}{\frac{I_{input}}{I'_{uniform}} - z} - \alpha_{half} \right) \middle/ c \right] \middle/ m + t_{half}$$
 (9)

where the values of constants were the same as those in Eq. (7).

We plotted t(z) with the initial etching time of 7.5 min at the tip (Fig. 3a). One should note that a lower initial etching time (i.e., lower attenuation coefficient) at the rod tip leads to a lower value for the uniform light scattering intensity (I'_{uiform}), thus a longer distance for light scattering under a constant I_{input} . Therefore, a potential method to scale up the uniform scattering distance through gradient etching is to apply a shorter initial etching time for the tip, indicating the necessity for using waveguides with fewer initial surface cracks. If the initial rod surface is very uniform, we could apply a shorter initial etching time for the tip. This way, the maximum distance of uniform etching can be enlarged. The governing function for gradient etching, Eq. (9), was then realized through Arduino coding, as detailed in the flow chart (Fig. 3b).

3.3. Uniform light scattering for gradient-etched waveguides and comparison with state-of-the-art activities

Light scattering exhibited different behaviors for gradient-etched, uniform-etched, and non-etched waveguides (Fig. 4a). The overall photon energy can be estimated by integrating the light intensities over the transmission distance. Compared with etched rods, non-etched ones almost had no light scattered out from the sides, proving the necessity for surface modification of waveguide-based systems. The overall photon energies along the whole waveguides were at similar levels for gradient-etched and uniform-etched rods, as indicated by their similar areas below the light distribution curves. This result underscores that while gradient etching did not change the overall photon energy, it enabled a more uniform photon energy distribution along the whole waveguide.

By applying different etching time to various locations of the waveguides, we formed a gradient distribution of surface roughness (i. e., attenuation coefficient), thus uniform light scattering profiles. We

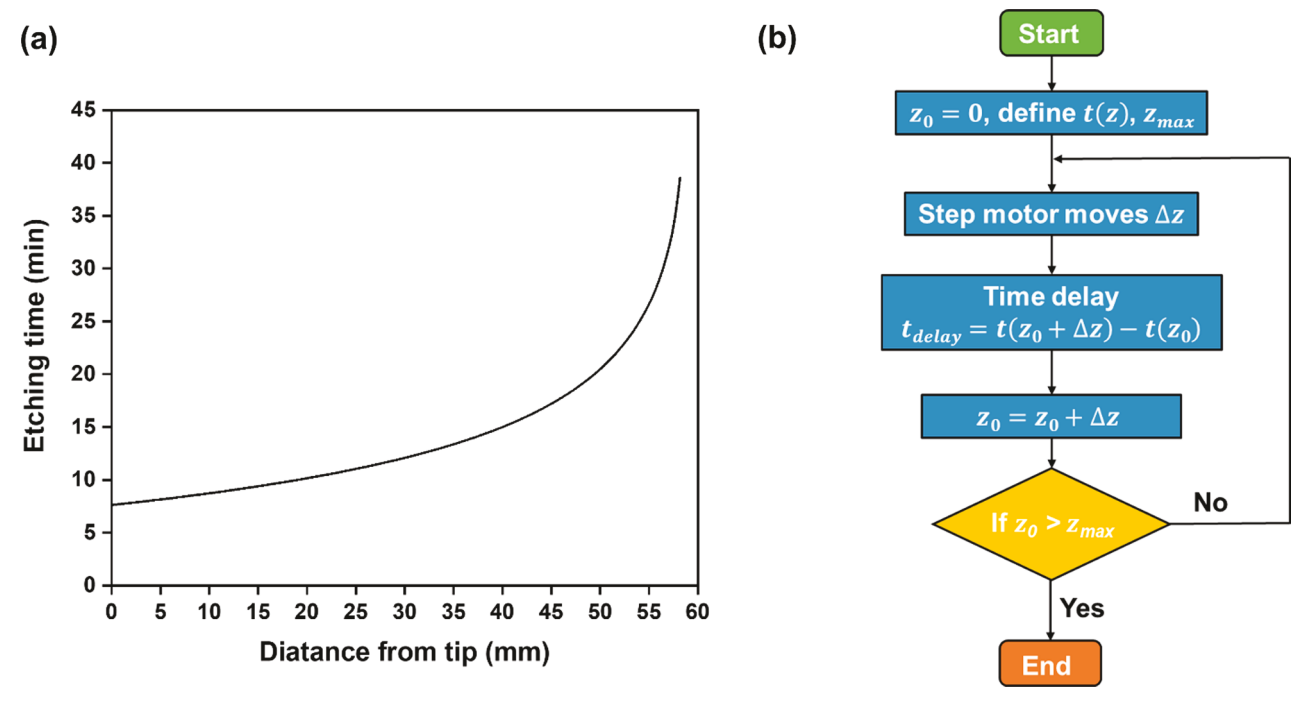


Fig. 3. (a) Etching time (*t*) as a function of the distance from the rod tip (*z*). The attenuation coefficient at z = 0 is set as 0.014 mm⁻¹. The etching time as a function of rod position t(z) is obtained by equaling $\alpha(z)$ and $\alpha(t)$. (b) Flow chart of the gradient etching process. The Arduino board controls the motion of the linear slider, which enables controlled etching for waveguides.

then applied the coefficient of variation (CV), a ratio of the standard deviation to the mean [31], to characterize the relative light distribution uniformity of different light scattering profiles.

For the 1 h uniform-etched rod, the CV for light intensity distribution was calculated to be 1.64 (Fig. 4a). The homogeneous surface properties under uniform etching led to exponential decay in scattering intensity distribution (Fig. 4b). For the gradient-etched rod, the scattering intensity was averaged as 3.0 W m⁻², with a slight increase towards the end, possibly due to tip light reflection (Figs. 4a, S2a). The CV was calculated as 0.12, a value more than 13 times lower than that of the uniform-etched rod (1.64), indicating an enhanced uniformity by at least 13 times. The uniform light distribution resulted from the gradient surface roughness distribution: a smoother surface closer to the light source and a rougher surface to the end (Fig. 4c). The etching time for the two ends for the gradient-etched rod was close to 7.5 min and 40 min, respectively, which accounted for the relatively lower surface roughness than under 1 h uniform etching (Figs. 4c, S2b). A zoomed-in comparison between different scattering decay profiles reveals that gradient etching significantly improved the photonic transport efficiency than non-etched rods (Fig. S2c) [1]. For the latter, the differences in refractive indexes between the quartz rod $(n_1 = 1.5)$ [2] and air $(n_2 =$ 1.0) [32] led to the dominant total internal reflection, and only a tiny amount of evanescent light was emitted. We envision advanced surface characterized techniques, such as the atomic force microscope (AFM), could be promising in guiding precision surface control.

A detailed comparison of light scattering profiles for the current study and the state-of-the-art methods for uniform light scattering by waveguides is summarized (Table S1). We compared gradient etching with tip coating, physical carving, and the adoption of engineered pillars. For the present study, the change in scattering intensity after half-length for the gradient-etched and 1 h uniform-etched rod was 11.3% and 97.4%, respectively. The coefficient of variation was 0.12 for the former and 1.64 for the latter. The result of uniform etching in the current work is comparable to a previous study [22]. They applied quartz optic fibers into an internal-illuminated monolith photoreactor and studied the sidelight emission properties. After half-length, the

intensity change for 0.5 mm outer diameter (OD), 1.0 mm OD, and 1.5 mm OD fibers was 97.0%, 92.8%, 86.6%, respectively. The coefficients of variation for the three conditions ranged from 1.21 to 2.02. Tip coating was studied by Liou et al. [21] as an approach to enhance scattered light amount but would not affect the light distribution uniformity (CV was \sim 0.53 before and after tip coating). They also studied the effect of different carving configurations on the scattering light distribution. They found that carving from the middle with increased depth could not only help slow down the intensity decay (49.3% intensity decrease after half-length with carving, compared with 66.2% decrease after half-length without carving), but also facilitated better light distribution (CV was 0.41 with carving, and was 0.53 without carving). However, the best uniformity achieved by physical carving was still more than 3.4 times lower than the gradient etching approach described in the current study. We also compared with applying uniform engineered pillars for waveguides. The CV values calculated for four measurements by the engineered pillar approach ranged between 0.63 and 0.94 [27]. These were all still less uniform than the gradient etching method presented herein, not to mention the high cost and complex equipment (i.e., the contact aligner) involved in applying engineered pillars.

3.4. Photodegradation activities for surface-engineered waveguide-based photocatalytic system

Fig. 5 shows a comparison of the methylene blue photodegradation activities for the photocatalytic system with non-etched, 1 h uniform-etched, gradient-etched waveguides. Compared with uniform-etched rods, gradient etching showed a $\sim\!\!4$ times improvement in degradation after 1 h of UV irradiation. We attributed this to the improved light distribution uniformity by gradient-etched designs (Fig. S2b). Moreover, the gradient-etched rod-based system exhibited a $\sim\!\!8$ times higher photodegradation rate than non-etched systems. This further verified the need to engineer surface roughness distributions for waveguide-based photocatalytic systems. The microscopic morphology of the catalyst material is shown in Fig. S3. We should note that while the

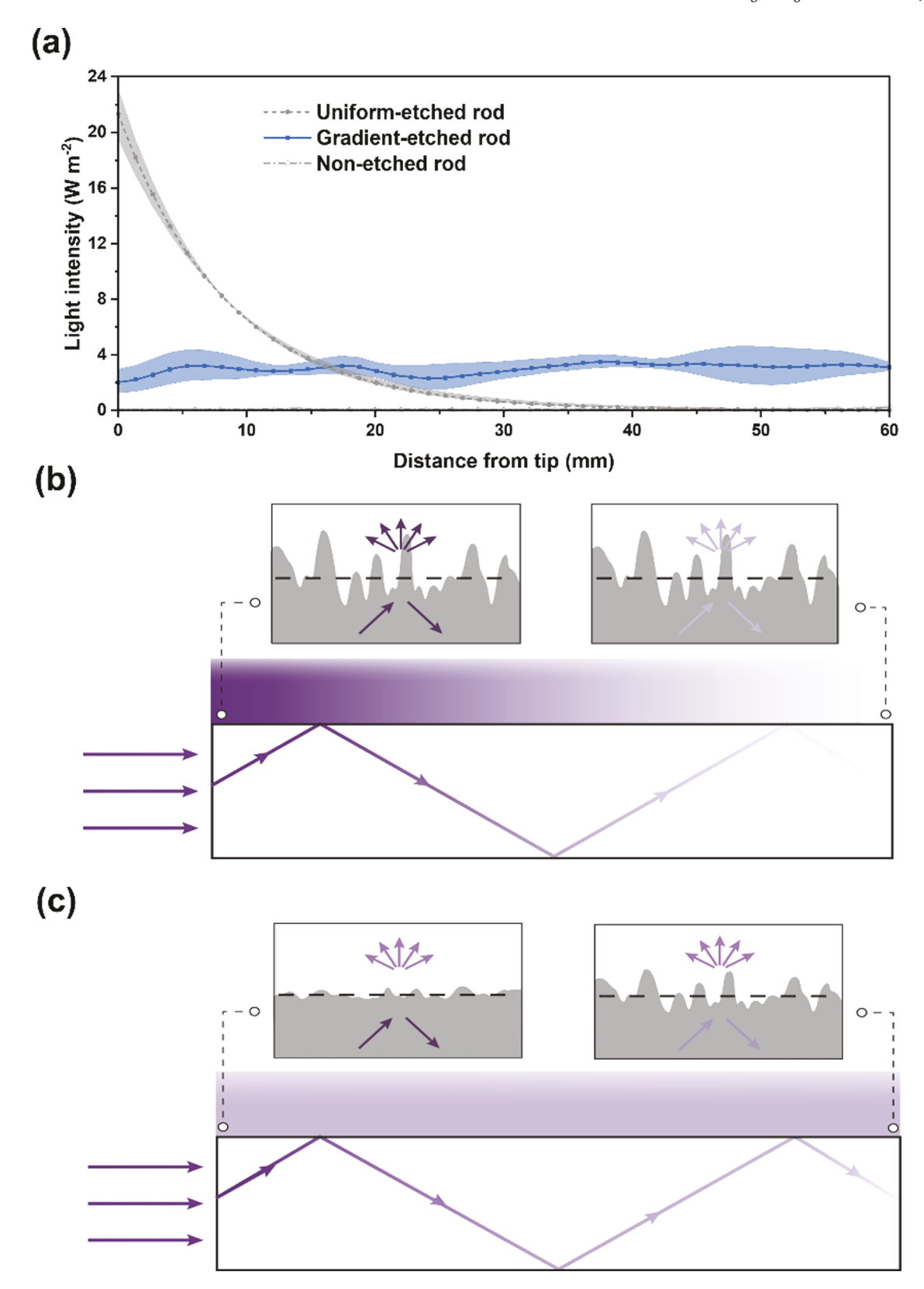


Fig. 4. (a) Light scattering profiles for 1 h uniform-etched, gradient-etched, and non-etched rods. Scattered light experiences exponential decay for uniformed etched rod (denoted by the solid gray circle). Gradient etching leads to uniform light scattering (denoted by the blue square). Non-etched rods rarely have light scattering (denoted by the hollow gray circle) due to total internal reflection. The shaded area indicates standard deviations calculated from three experiments. (b) Schematics for the change in light scattering for 1 h uniform-etched rod along the transmission. From left to right, surface roughness keeps constant, and light scattering intensity experiences exponential decay. (c) Schematics for the change in light scattering for the gradient-etched rod. From left to right, surface roughness exhibits a gradient increase, and light scattering intensity keeps constant (For interpretation of the references to color in this figure legend, the reader is referred to the web version of this article.).

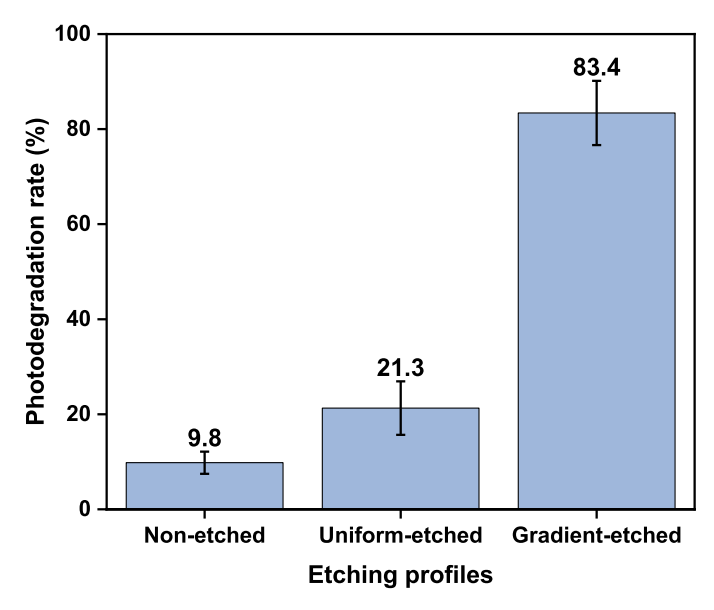


Fig. 5. Comparison of methylene blue photodegradation activities for a photocatalytic system with non-etched, $1\ h$ uniform-etched, gradient-etched waveguides.

current study only examined the application of surface-engineered waveguides for room-temperature photodegradation of methylene blue, we have previously [4] validated that waveguide-based systems could also work for high-temperature applications such as gas-phase photocatalytic reduction of CO₂. With the incorporation of waveguide surface engineering demonstrated here, we envision the photocatalytic efficiency can be further increased. Since waveguides are made of quartz (SiO₂) with a melting point of $\sim 1700~^{\circ}$ C, those systems can well withstand harsh operating conditions (pressure and temperature), as long as other components (e.g., reactor body, connecting tubes) are made of suitable materials that can work under those conditions.

Here, we used methylene blue photodegradation as a simple case study to prove that waveguide surface engineering enabled uniform light distribution, leading to improved performance for a photocatalytic system. More photocatalytic tests need to be conducted to guide waveguide engineering. Some future directions include how various factors such as light irradiation orientations (e.g., top illumination, side illumination) and irradiation methods (e.g., LEDs, direct use of solar) will affect the waveguide system design.

4. Conclusions

In summary, we successfully built two low-cost linear-slider-based platforms for continuous light measurement and controlled chemical etching. We applied different etching durations to different waveguide locations so that a gradient surface roughness distribution was forged for uniform light scattering. The coefficient of variation comparison validated gradient etching as a valid method to increase light distribution uniformity, with improved performance compared with state-of-the-art approaches (e.g., tip coating, physical carving, engineered pillars, etc.). We also evaluated the effect of different waveguide configurations in a photocatalytic test for methylene blue degradation. Photodegradation activity with gradient-etched waveguides was ~4 times higher than uniform-etched designs and ~8 times higher than non-etched ones. This study underscores controlled surface etching for waveguides as a viable approach for concurrently optimizing light delivery and catalyst availability to maximize photocatalytic reaction rates.

CRediT authorship contribution statement

Xiangkun Elvis Cao: Conceptualization, Funding acquisition, Investigation, Data curation, Formal analysis, Writing – original draft, Writing – review & editing. **Tao Hong:** Investigation, Data curation, Formal analysis, Writing – review & editing. **Spencer Hong:** Formal analysis, Writing – review & editing. **David Erickson:** Conceptualization, Funding acquisition, Supervision, Writing – review & editing.

Declaration of Competing Interest

D.E. has an equity interest in Dimensional Energy – a company focused on commercializing the ${\rm CO}_2$ to fuel research using a photothermal catalytic reactor platform.

Acknowledgments

This work was supported by the National Science Foundation STTR Award 1720824 & 1831166, the Scale Up and Prototyping Award, and the Bill Nye '77 Award from the Engineering Learning Initiatives at the College of Engineering of Cornell University.

Supplementary materials

Supplementary material associated with this article can be found, in the online version, at doi:10.1016/j.ceja.2021.100192.

References

- [1] N.J. Peill, M.R. Hoffmann, Development and optimization of a TiO₂-coated fiber-optic cable reactor: photocatalytic degradation of 4-chlorophenol, Environ. Sci. Technol. 29 (12) (1995) 2974–2981, https://doi.org/10.1021/es00012a013.
- [2] H. 'O'Neal Tugaoen, S. Garcia-Segura, K. Hristovski, P. Westerhoff, Compact light-emitting diode optical fiber immobilized TiO₂ reactor for photocatalytic water treatment, Sci. Total Environ. 613-614 (2018) 1331–1338, https://doi.org/10.1016/j.jerictory.2017.09.242
- [3] M.R. Hoffmann, S.T. Martin, W. Choi, D.W. Bahnemann, Environmental applications of semiconductor photocatalysis, Chem. Rev. 95 (1) (1995) 69–96, https://doi.org/10.1021/cr00033a004.
- [4] X.E. Cao, Y. Kaminer, T. Hong, P. Schein, T. Liu, T. Hanrath, D. Erickson, HI-light: a glass waveguide based "shell-and-tube" photothermal reactor platform for converting Co₂ to fuels, iScience 23 (12) (2020), 101856, https://doi.org/ 10.1016/j.jcsi.2020.101856
- [5] X. Cao, T. Hong, T. Liu, J. Akemi, T. Hanrath, D. Erickson, A scalable glass waveguide-based optofluidic photoreactor for converting CO₂ to fuels, in: Proceedings of the Integrated Optics: Devices, Materials, and Technologies XXIV 11283, 2020, 112831N, https://doi.org/10.1117/12.2546536.
- [6] X. Cao, T. Hong, T. Liu, D. Erickson, Engineering the glass waveguide surface for uniform light refraction inside an optofluidic photoreactor, in: Proceedings of the MOEMS and Miniaturized Systems XIX 11293, 2020, 112930E, https://doi.org/ 10.1117/12.2546554.
- [7] X. Liu, X.E. Cao, Y. Liu, X. Li, M. Wang, M. Li, Branched multiphase TiO₂ with enhanced photoelectrochemical water splitting activity, Int. J. Hydrog. Energy 43 (46) (2018) 21365–21373, https://doi.org/10.1016/j.ijhydene.2018.09.193.
- [8] L. Wang, M. Xia, H. Wang, K. Huang, C. Qian, C.T. Maravelias, G.A. Ozin, Greening ammonia toward the solar ammonia refinery, Joule 2 (6) (2018) 1055–1074, https://doi.org/10.1016/j.joule.2018.04.017.
- [9] D.F.R. Doud, L.T. Angenent, Toward electrosynthesis with uncoupled extracellular electron uptake and metabolic growth: enhancing current uptake with Rhodopseudomonas palustris, Environ. Sci. Technol. Lett. 1 (9) (2014) 351–355, https://doi.org/10.1021/ez500244n.
- [10] D.F.R. Doud, A. Jain, S.S. Ahsan, D. Erickson, L.T. Angenent, *In situ* UV disinfection of a waveguide-based photobioreactor, Environ. Sci. Technol. 48 (19) (2014) 11521–11526, https://doi.org/10.1021/es502812k.
- [11] E.E. Jung, A. Jain, N. Voulis, D.F.R. Doud, L.T. Angenent, D. Erickson, Stacked optical waveguide photobioreactor for high density algal cultures, Bioresour. Technol. 171 (2014) 495–499, https://doi.org/10.1016/j.biortech.2014.08.093.
- [12] S.S. Ahsan, A. Gumus, A. Jain, L.T. Angenent, D. Erickson, Integrated hollow fiber membranes for gas delivery into optical waveguide based photobioreactors, Bioresour. Technol. 192 (2015) 845–849, https://doi.org/10.1016/j. biortech.2015.06.028.
- [13] Y. Dong, P. Duchesne, A. Mohan, K.K. Ghuman, P. Kant, L. Hurtado, U. Ulmer, J.Y. Y. Loh, A.A. Tountas, L. Wang, A. Jelle, M. Xia, R. Dittmeyer, G.A. Ozin, Shining light on CO₂: from materials discovery to photocatalyst, photoreactor and process engineering, Chem. Soc. Rev. 49 (16) (2020) 5648–5663, https://doi.org/10.1039/d0cs00597e.

- [14] J.Y.Y. Loh, A. Mohan, A.G. Flood, G.A. Ozin, N.P. Kherani, Waveguide photoreactor enhances solar fuels photon utilization towards maximal optoelectronic – photocatalytic synergy, Nat. Commun. 12 (1) (2021), https://doi. org/10.1038/s41467-020-20613-2.
- [15] D. Erickson, D. Sinton, D. Psaltis, Optofluidics for energy applications, Nat. Photonics 5 (10) (2011) 583–590, https://doi.org/10.1038/Nphoton.2011.209.
- [16] A. Jain, N. Voulis, E.E. Jung, D.F.R. Doud, W.B. Miller, L.T. Angenent, D. Erickson, Optimal intensity and biomass density for biofuel production in a thin-light-path photobioreactor, Environ. Sci. Technol. 49 (10) (2015) 6327–6334, https://doi. org/10.1021/es5052777.
- [17] L.W. Miller, M.I. Tejedor-Tejedor, M.A. Anderson, Titanium dioxide-coated silica waveguides for the photocatalytic oxidation of formic acid in water, Environ. Sci. Technol. 33 (12) (1999) 2070–2075, https://doi.org/10.1021/es980817g.
- [18] M. Lanzarini-Lopes, B. Cruz, S. Garcia-Segura, A. Alum, M. Abbaszadegan, P. Westerhoff, Nanoparticle and transparent polymer coatings enable UV-C sideemission optical fibers for inactivation of escherichia coli in water, Environ. Sci. Technol. 53 (18) (2019) 10880–10887, https://doi.org/10.1021/acs.est.9b01958.
- [19] Y. Özbakır, A. Jonáš, A. Kiraz, C. Erkey, An aerogel-based photocatalytic microreactor driven by light guiding for degradation of toxic pollutants, Chem. Eng. J. 409 (2021), 128108, https://doi.org/10.1016/j.cej.2020.128108.
- [20] C. Boyle, N. Skillen, L. Stella, P.K.J. Robertson, Development and optimization of an immobilized photocatalytic system within a stacked frame photoreactor (SFPR) using light distribution and fluid mixing simulation coupled with experimental validation, Ind. Eng. Chem. Res. 58 (8) (2019) 2727–2740, https://doi.org/ 10.1021/acs.jecr.8b05709.
- [21] P.Y. Liou, S.C. Chen, J.C.S. Wu, D. Liu, S. MacKintosh, M. Maroto-Valer, R. Linforth, Photocatalytic CO₂ reduction using an internally illuminated monolith photoreactor, Energy Environ. Sci. 4 (4) (2011) 1487–1494, https://doi.org/ 10.1039/c0ee00609b.
- [22] K.T. Lu, V.H. Nguyen, Y.H. Yu, C.C. Yu, J.C.S. Wu, L.M. Chang, A.Y.C. Lin, An internal-illuminated monolith photoreactor towards efficient photocatalytic

- degradation of ppb-level isopropyl alcohol, Chem. Eng. J. 296 (2016) 11–18, https://doi.org/10.1016/j.cej.2016.03.097.
- [23] B. Tahir, M. Tahir, N.S. Amin, Performance analysis of monolith photoreactor for CO₂ reduction with H₂, Energy Convers. Manag. 90 (2015) 272–281, https://doi. org/10.1016/j.enconman.2014.11.018.
- [24] F. Denny, J. Scott, G.D. Peng, R. Amal, Channelled optical fibre photoreactor for improved air quality control, Chem. Eng. Sci. 65 (2) (2010) 882–889, https://doi. org/10.1016/j.ces.2009.09.038.
- [25] N.J. Peill, M.R. Hoffmann, Mathematical model of a photocatalytic fiber-optic cable reactor for heterogeneous photocatalysis, Environ. Sci. Technol. 32 (3) (1998) 398–404, https://doi.org/10.1021/es960874e.
- [26] R.E. Marinangeli, D.F. Ollis, Photoassisted heterogeneous catalysis with optical fibers: I. Isolated single fiber, AIChE J. 23 (4) (1977) 415–426, https://doi.org/ 10.1002/aic.690230403.
- [27] S.S. Ahsan, B. Pereyra, E.E. Jung, D. Erickson, Engineered surface scatterers in edge-lit slab waveguides to improve light delivery in algae cultivation, Opt. Express 22 (21) (2014) A1526–A1537, https://doi.org/10.1364/Oe.22.0a1526.
- [28] S.S. Ahsan, A. Gumus, D. Erickson, Stacked waveguide reactors with gradient embedded scatterers for high-capacity water cleaning, Opt. Express 23 (24) (2015) A1664, https://doi.org/10.1364/oe.23.0a1664.
- [29] S. Torkamani, S.N. Wani, Y.J. Tang, R. Sureshkumar, Plasmon-enhanced microalgal growth in miniphotobioreactors, Appl. Phys. Lett. 97 (4) (2010), 043703, https://doi.org/10.1063/1.3467263.
- [30] A.K. Ray, Design, modelling and experimentation of a new large-scale photocatalytic reactor for water treatment, Chem. Eng. Sci. 54 (15–16) (1999) 3113–3125, https://doi.org/10.1016/s0009-2509(98)00507-7.
- [31] A. Brunsting, P.F. Mullaney, Differential light scattering from spherical mammalian cells, Biophys. J. 14 (6) (1974) 439–453, https://doi.org/10.1016/s0006-3495(74)
- [32] P.E. Ciddor, Refractive index of air: new equations for the visible and near infrared, Appl. Opt. 35 (9) (1996) 1566–1573, https://doi.org/10.1364/AO.35.001566.